



Growth behavior of fatigue cracks in ultrafine grained Cu smooth specimens with a small hole

Masahiro Goto, Kakeru Morita, Junichi Kitamura, Takaei Yamamoto, Masataka Baba

Department of Mechanical Engineering, Oita University, Japan.

masagoto@oita-u.ac.jp, v14e1035@oita-u.ac.jp, junichi@oita-u.ac.jp, tyama@oita-u.ac.jp, v14e1025@oita-u.ac.jp

Seung-zeon Han

Materials Engineering Department, Korea Institute of Materials Science, Republic of Korea.

szehan@kims.re.kr

Sangshik Kim

Department of Metallurgical and Materials Engineering, Gyeongsang National University, Republic of Korea.

sang@gnu.ac.kr

ABSTRACT. In order to study the growth mechanism of fatigue cracks in ultrafine grained copper, stress-controlled fatigue tests of round-bar specimens with a small blind hole as a crack starter were conducted. The hole was drilled on the surface where an intersection between the shear plane of the final ECAP processing and the specimen surface makes an angle of 45° or 90° with respect to the loading axis. At a low stress ($\sigma_a = 90$ MPa), the direction of crack paths was nearly perpendicular to the loading direction regardless of the location of the hole. Profile of crack face was examined, showing the aspect ratio (b/a) of $b/a = 0.82$. At a high stress ($\sigma_a = 240$ MPa), although the growth directions inclined 45° and 90° to the loading-axis were observed depending on the location of the drilling hole, crack faces in these cracks were extended along one set of maximum shear stress planes, corresponding to the final ECAP shear plane. The value of aspect ratios was $b/a = 0.38$ and 1.10 for the cracks with 45° and 90° inclined path directions, respectively. The role of deformation mode at the crack tip areas on crack growth behavior were discussed in terms of the mixed-mode stress intensity factor. The crack path formation at high stress amplitudes was affected by the in-plane shear-mode deformation at the crack tip.

KEYWORDS. Fatigue; Ultrafine grain; Copper; Crack propagation; Grain coarsening; Stress intensity factor.

INTRODUCTION

Equal channel angular pressing (ECAP) is currently used to obtain grains down to the submicron level, which are tenfold to hundredfold finer than conventional materials. Until recently, most studies have focused on optimizing processing conditions, underlying microstructural mechanisms, or attainable post-ECAP strength levels [1-4]. For



envisaged structural applications of ultrafine grained (UFG) metals, attention has been paid to fatigue performance. Studies of fatigue on UFG materials processed by ECAP has been focused mainly on cyclic deformation, S-N plots, formation of shear bands (SBs) and underlying microstructural mechanisms [5-11].

Since the fatigue life of machine components and structures is mainly controlled by the growth life of a fatigue crack, the crack growth behavior should be clarified for the design of safe machine components and structures. Recently, in the high-cycle fatigue (HCF) tests, the growth behaviors of long (millimeter-range) cracks in UFG metals [12-16] were studied for compact-tension, single edge-notched, single edge bend and center-cracked tensile specimens. With regard to the growth characteristics of long fatigue cracks in UFG materials, the higher growth rates in low and medium values of the stress intensity factor (SIF) range and the lower growth thresholds have been reported. These phenomena appear to be attributed to the weakened roughness-induced crack closure caused by the much smoother fracture surface and lower deflection of the crack path. The smoother crack-path/fracture-surface is caused by decreased grain sizes and limited crack tip plasticity.

It has been shown that the crack growth life from an initial size to 1 mm accounted for about 70% of the fatigue life of plain specimens of many conventional grain-sized metals [17, 18]. Therefore, the growth behavior of small cracks must be clarified to estimate the fatigue life of smooth members. Regarding the crack growth in strain-controlled low-cycle fatigue (LCF) tests and stress-controlled fatigue tests at high stress amplitudes corresponding to LCF regime, study on fatigue crack growth mechanism has been relatively rare, and only a few reports can be found [19, 20]. Meanwhile, for ECAPed samples, the $y\text{-}z$ -, $x\text{-}z$ -, and xy -planes are defined by three mutually orthogonal sectioning planes that are perpendicular to the longitudinal axis of the pressed sample, parallel to the sample side, and parallel to the sample top faces at the point of exit from the die, respectively. In strain-controlled LCF tests, SBs in the $x\text{-}z$ -plane were oriented at 45° to the loading axis parallel to the longitudinal axis of the pressed samples, while those in the xy -plane were nearly perpendicular to the loading axis [21]. The SBs appear on the $x\text{-}z$ -plane at 45° to the loading direction mainly because it is the plane of maximum resolved shear stress [22]. Fatigue cracks were initiated in and propagated along these SBs. Consequently, the LCF crack on the $x\text{-}z$ -plane grew along the direction inclined at 45° to the loading axis. Up to now, LCF crack growth behavior of UFG materials have been mainly discussed from the viewpoints of microstructure and morphological features of surface damage. On the other hand, the discussion from the mechanical viewpoints should be done for a better understanding of the fatigue damage of UFG materials. However, such studies are few and certain questions remain unanswered.

The objective of this study is to investigate the physical background of the formation mechanism of crack growth paths in the HCF and LCF regimes in terms of the mixed-mode deformation at the crack tip.

EXPERIMENTAL PROCEDURES

Pure oxygen-free copper (99.99 wt% Cu) was used in the experiment. Prior to ECAP processing, the samples were annealed at 500°C for 1 h (average grain size: $100\ \mu\text{m}$). The ECAP die had a 90° angle between intersecting channels. The angles at the inner and outer corners of the channel intersection in the die were 90° and 45° , respectively. Repetitive ECAP was accomplished according to the Bc route (after each pressing, the billet bar was rotated 90° around its longitudinal axis). Eight extrusion passes resulted in an equivalent shear strain of approximately 7.8. The microstructure of an ECAP rod obtained using a transmission electron microscope showed fine equiaxed grains of approximately 300-nm diameter and large elongated grains.

Fatigue specimens 5 mm in diameter were machined from their respective processed bars. Although the specimens had shallow circumferential notches (20-mm notch radius and 0.25-mm notch depth), the fatigue strength reduction factor for this geometry was close to 1, meaning that they could be considered plain. The fatigue specimens were electrolytically polished (approximately $\approx 25\ \mu\text{m}$ from the surface layer) prior to mechanical testing to remove any preparation-affected surface layer. Polishing was carried out at 25°C using an electrolyte consisting of 600 mL of phosphoric acid, 300 mL of distilled water, and 100 mL of sulfuric acid. Prior to testing, a small blind hole (both diameter and depth of 0.1 mm) was drilled as a crack starter on the middle surfaces of the plain specimens. Fig. 1 shows the location of the drilling hole. A hole was drilled on the surface where an intersection between the shear plane of the final pressing and the specimen surface makes an angle of 45° ($x\text{-}z$ -plane) or 90° (xy -plane) with respect to the loading axis. All fatigue tests were performed at room temperature using a rotating-bending fatigue machine (constant bending-moment type) operating at 50 Hz. The fatigue damage on the specimen surface was observed using an optical microscope (OM) and a scanning electron microscope (SEM). The crack length, l , was measured along the circumferential direction of the surface. The



crack length was measured using a plastic replication technique. The stress value referred to is that of the nominal stress amplitude, σ_a , at the minimum cross-section (5-mm diameter).

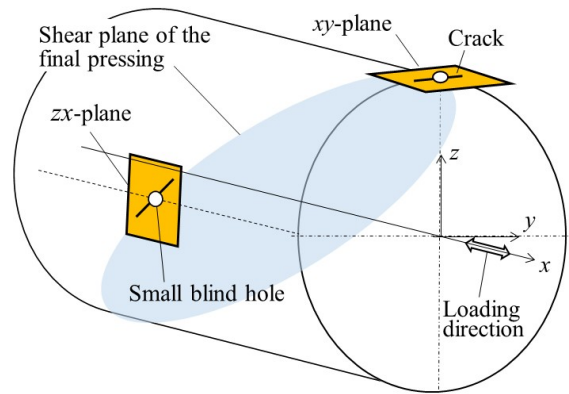


Figure 1: Illustration showing the location of the drilled hole as a crack starter, and the shear plane of the final ECAP pressing.

The distribution of the grain sizes and grain boundary misorientation were determined by electron backscatter diffraction (EBSD) analysis. The specimens were ground using silicon carbide papers and polished with polycrystalline 3- and 1- μm diamond suspension. Final polishing was performed using a 0.04- μm colloidal silica suspension for 30–60 min. EBSD mappings were executed using a Tescan Mira II SEM incorporating an EDAX-TSL Hikari EBSD detector. Each hexagonally shaped pixel was 40 nm for the UFG copper samples and 1.0 μm for the conventional grain-sized copper samples. Orientation imaging microscopy analysis software version 5.3 was used to analyze the orientation characteristics and misorientation distributions.

EXPERIMENTAL RESULTS

Figure 2 shows the crack growth paths in the zx - and xy -planes under high and low stress amplitudes ($\sigma_a = 240$ and 90 MPa). The surface-cracks within the zx - and xy -planes are referred to hereafter as the “ zx -plane crack” and “ xy -plane crack”, respectively. At $\sigma_a = 240$ MPa, the zx -plane crack that initiated from the hole created a 45° incline to the loading axis and this crack path direction was parallel to the shear direction of the final ECAP processing (Fig. 1). The 45° inclined crack growth direction has been commonly observed in the zx -plane of LCF UFG metals [20, 21, 23]. However, the xy -plane crack grew nearly perpendicular to the loading axis like crack paths in conventional grain-sized materials. At $\sigma_a = 90$ MPa, on the other hand, the macroscale growth direction was perpendicular to the loading axis regardless of the plane where the crack initiated; nevertheless, the crack propagated in a zigzag manner at the microscale.

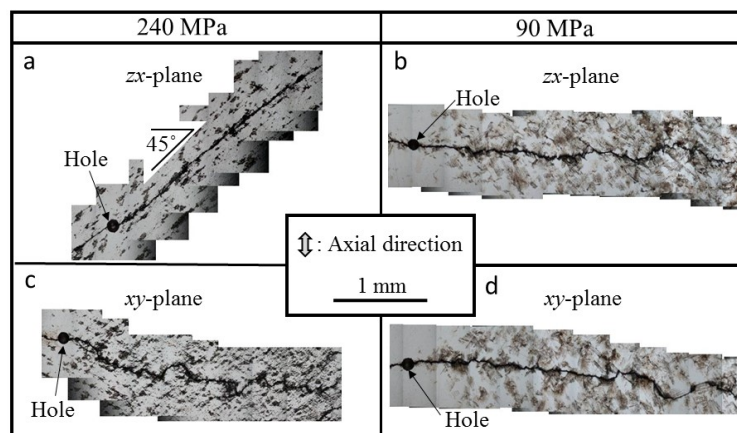


Figure 2: Effect of stress amplitudes on crack growth paths in the zx - and xy planes: (a, and b) the zx -plane crack at $\sigma_a = 240$ and 90 MPa; (c and d) the xy -plane crack at $\sigma_a = 240$ and 90 MPa.

The SEM micrograph in Fig. 3a shows the post-fatigued surface at repeated stressing of $\sigma_a = 240$ MPa. A high population of SBs was observed over the whole surface of the specimen. The SBs initiated along the shear plane of the final ECAP processing, and their lengths were less than ten micrometers. On the other hand, the post-fatigued surface formed under $\sigma_a = 90$ MPa (Fig. 3b) had slip-band like traces greater than a few tens of micrometers. The difference in formation mechanism of surface damage between high and low stress amplitudes should affect the formation mechanisms of crack paths under high and low stresses.

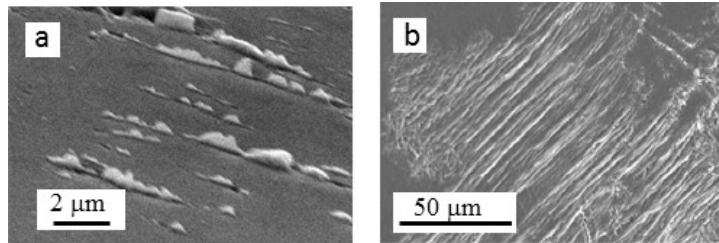


Figure 3: SEM micrographs of damaged traces in the post-fatigued specimens: (a) SBs at $\sigma_a = 240$ MPa ($N_f = 1.95 \times 10^5$); (b) slip band like traces at $\sigma_a = 90$ MPa ($N_f = 1.33 \times 10^7$).

To study the crack growth path inside the specimen fatigued at high and low stress amplitudes, the specimens were sectioned in the longitudinal direction (parallel to the x -axis), at specific crack lengths (Figs. 4 and 5), followed by etching of the sectioned planes. Figs. 4b and 4d show the crack growth path formed at $\sigma_a = 240$ MPa in the sectioned plane for the zx - and xy -plane crack, respectively. The inner growth direction of the zx -plane crack was perpendicular to the specimen surface (zx -plane). For the xy -plane crack, although the inner growth direction just after the initiation was nearly perpendicular to the loading axis, the crack gradually changed its direction to the plane inclined 45° to the specimen surface (xy -plane). Although the inclination direction of the crack path to the loading axis was different between the zx - and xy -plane cracks, the paths for both cracks were parallel to the shear plane of the final ECAP pressing (Fig. 1), except for the initial growth path in the xy -plane crack. Figs. 5b and 5d show the crack growth path formed at $\sigma_a = 90$ MPa in the sectioned plane for the zx - and xy -plane crack, respectively. The crack growth paths for both planes were vertical to the specimen surface. The vertical growth path was commonly observed in the conventional grain-sized materials.

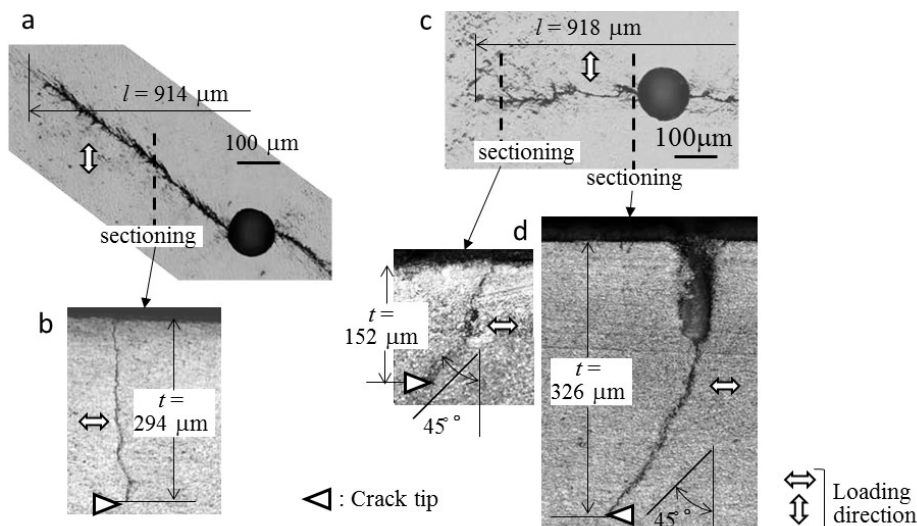


Figure 4: Crack paths at $\sigma_a = 240$ MPa: (a and c) sectioning position described in the crack paths of the zx - and xy -planes; (b and d) crack paths in the sectioned plane for the zx - and xy -plane cracks.

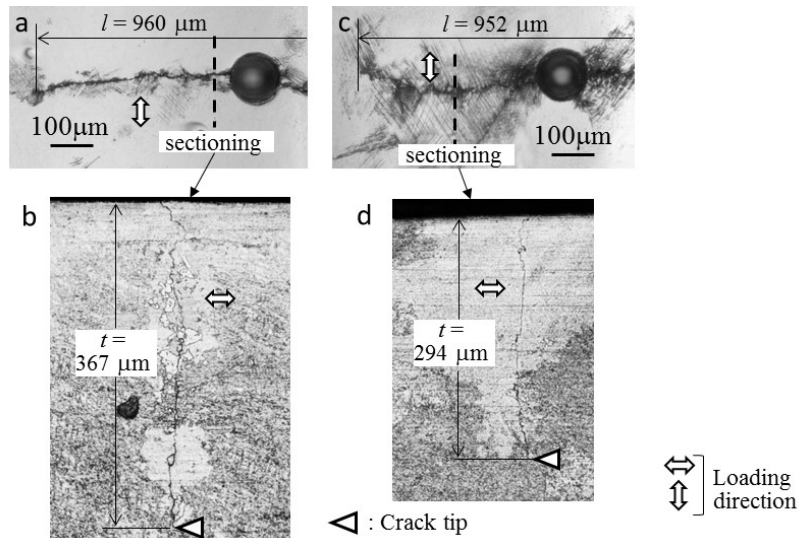


Figure 5: Crack paths at $\sigma_a = 90$ MPa: (a and c) sectioning position described in the crack paths of the zx - and xy -planes; (b and d) crack paths in the sectioned plane for the zx - and xy -plane cracks.

Fig. 6 shows the profile of the crack face, y/l or z/l versus t/l relationship. Dashed lines in Fig. 6a are the crack face profile at $\sigma_a = 240$ MPa represented in terms of T/L , where, l and L are the crack length measured along the circumferential direction at the specimen surface, and along the crack path direction, respectively, and t and T are the crack depth measured along the vertical direction to the specimen surface, and along the crack face direction, respectively (Figs. 7a and 7b). Here, for the xy -plane crack, the flat crack face/path illustrated in Fig. 7b was assumed, whereas the actual path was slightly curved, especially in the initial growth stage. The values of t/l and T/L at the deepest point were

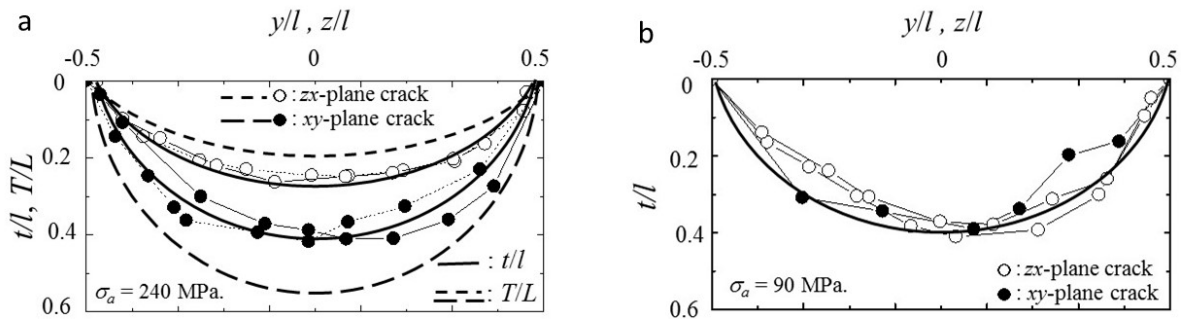


Figure 6: Profile of the crack face in terms of dimensionless sizes: (a) $\sigma_a = 240$ MPa; (b) $\sigma_a = 90$ MPa.

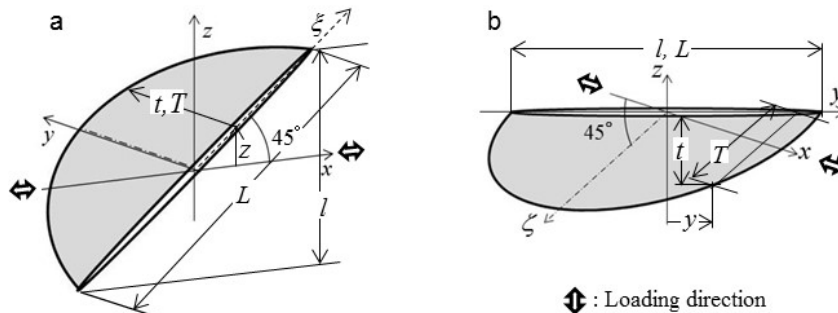


Figure 7: Definition of the crack length/depth for inclined cracks: (a) the zx -plane crack; (b) the xy -plane crack.



0.266 and 0.189 for the $\bar{x}\bar{x}$ -plane crack, and 0.389 and 0.550 for the $\bar{x}\bar{y}$ -plane crack, respectively. Fig. 6b shows the crack face profile at $\sigma_a = 90$ MPa. There was no significant difference in the crack face shape between the $\bar{x}\bar{x}$ - and $\bar{x}\bar{y}$ -plane cracks. The value of $t/l (= T/L)$ at the deepest point was 0.41 for both planes.

DISCUSSION

UFG materials processed by SPD techniques have non-equilibrium microstructures [24, 25] with limited thermal and mechanical stability. Such non-equilibrium microstructures can easily change properties under applied cyclic stressing at a certain temperature. Remarkable levels of grain coarsening as the result of dynamic recrystallization have generally occurred in post-fatigued high-purity UFG copper [26, 27], whereas it has been shown that no grain coarsening occurred in cyclically deformed UFG copper [23, 28]. To study the grain growth as a result of cyclic stressing, EBSD analysis of the post-fatigued specimens was conducted. In order to conduct EBSD analysis of the post-fatigued microstructure just under the specimen surfaces, 0.15 mm surface layers of the post-fatigued round bar specimens were polished off to make a flat surface for EBSD analysis. The procedure for making the flat surface and the area analysed by EBSD are shown in a previous work [20]. Fig. 8a shows inverse pole figure (IPF) maps and grain boundary (GB) map of a post-ECAP sample (pre-fatigue) in the $\bar{x}\bar{x}$ -plane. Figs. 8b and 8c show the microstructure after a constant stressing of $\sigma_a = 240$ and 90 MPa, respectively. The GBs in the GB maps are denoted either by red lines corresponding to low angle GBs (LAGBs) where the misorientation, θ , is between 2° and 15° or by black lines corresponding to high angle GBs (HAGBs) with $\theta > 15^\circ$. The IPF maps for the post-fatigued sample indicates the development of subgrains within elongated grains, isolated with LAGBs. Image quality maps [27] showed that the microstructure in post-ECAP copper has enhanced strain energy due to the redundant defect structure, and the microstructure was therefore in the process of evolving to equiaxed grains isolated with HAGBs. The post-fatigue microstructure subjected to the constant stressing experienced grain coarsening, but the coarse grain sizes depended on the applied stress amplitudes. At high stress amplitude of $\sigma_a = 240$ MPa, coarse grains evolved from 1 to a few μm (Figs. 8b). No significant difference in coarse grain sizes between the $\bar{x}\bar{x}$ - and $\bar{x}\bar{y}$ -planes was observed. At $\sigma_a = 90$ MPa, long-term repetitions produced large coarse grains in excess of several tens of micrometres (Fig. 8c). Like the $\bar{x}\bar{x}$ -plane, large coarse grains were observed in the $\bar{x}\bar{y}$ -plane fatigued at $\sigma_a = 90$ MPa. Accordingly, it should be concluded that the damaged traces greater than a few tens of micrometers initiated at a low stress (Fig. 3b) were slip-bands formed in the coarse grains generated as a result of dynamic recrystallization. Regarding SB formation in the LCF regime, many investigators have observed morphological features and microstructure of SBs, discussing the formation mechanism of SBs in conjunction with the grain coarsening. However, clear evidence for an SB formation in UFG copper is still lacking, there are opposite views; for example, i) in ref.[26], the mechanism responsible for the SB formation was found to be the interaction of cyclically induced cell/grain coarsening, which led to strain localization, and ii) no grain coarsening occurred in cyclically deformed UFG copper (99.9% Cu [23]), and the coordinating GB sliding along the shear plane of the last ECAP pass could be the decisive mechanism in SB formation. The role of grain coarsening on the formation of SBs have been under discussion for a long time and are still awaiting final answers.

Regarding the crack paths, at low stress amplitudes (HCF regime), the growth direction of fatigue cracks in UFG copper was perpendicular to both the surface and loading direction regardless of the initiation site of cracks. There was no effect of microstructural inhomogeneity resulted from ECAP processing on the crack growth direction. This was because of the grain coarsening. As a result of generation of dynamically recrystallized coarse grains, the inhomogeneity of matrix caused by the ECAP processing is likely to disappear, giving rise to the macroscale growth-path perpendicular to both the specimen surface and loading direction. Accordingly, like conventional grain-sized materials, the crack at low stresses propagates via the striation formation mechanism [27], which is associated with crack tip retardation and blunting. However, the crack growth direction in the LCF regime (high stress amplitudes) was different from that in the HCF regime. In order to investigate the physical background of the unique crack growth directions at high stress amplitudes from the viewpoints of the deformation mode at the crack tip, the SIF values were evaluated, by assuming a semi-infinite body with inclined semi-elliptical surface cracks, subjected to tension stress in the x -direction at infinity. The applied tension stress is resolved into two stress components perpendicular and tangential to the crack face. Accordingly, a 45° inclined surface crack is subjected to both normal, $\sigma (= 1)$, and shear stress, $\tau (= 1)$, as illustrated in Figs. 9a and 9b. Noda et al. [29] analysed the SIFs of a semi-elliptical surface-crack subjected to modes I, II and III loading. The values of dimensionless SIF (DL-SIF), F_I , F_{II} , F_{III} , for the current surface-crack were taken from Noda's solution calculated for Poisson's ratio: $\nu = 0.3$. The DL-SIF, $F_I(\alpha)$, $F_{II}(\alpha)$, $F_{III}(\alpha)$, were defined as;

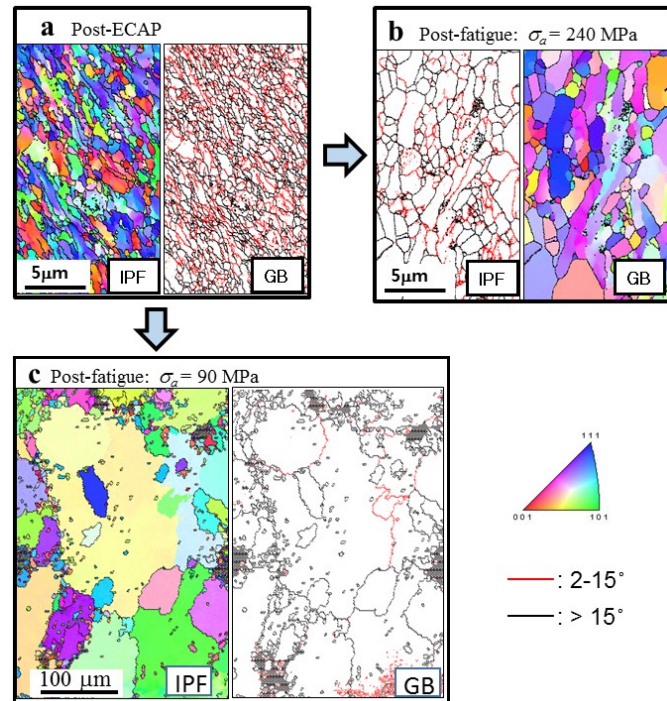


Figure 8: Orientation Imaging Microscopy orientation for sub-surface microstructure in the ξx -plane: (a) original microstructure before stressing; (b) after constant stressing at $\sigma_a = 240$ MPa; (c) after constant stressing at $\sigma_a = 90$ MPa

$$F_i(\alpha) = K_i(\alpha)/K_E(\alpha) \quad i = I, II, III \quad (1)$$

where, $K_i(\alpha)$ is SIF along the crack front and $K_E(\alpha)$ is SIF of an elliptical crack [29]. The location along a crack front was defined by the eccentric angle of the ellipse, α , defined as the angle for mapping a semi-circle illustrated with a dashed line in Fig. 9c. Namely, the actual position of a semi-elliptical crack at a given α value in Fig. 9c is indicated by a point A for the ξx -plane crack ($b < a$), and point B for the ξy -plane crack ($a < b$). Here, a and b are the half lengths and depth of a semi-elliptical crack measured along the crack face, respectively (Fig. 9c). The crack front at the surface and the deepest point are shown by $\alpha = 0$ and 90° , respectively. However, the DL-SIF values at the surface were evaluated by the values

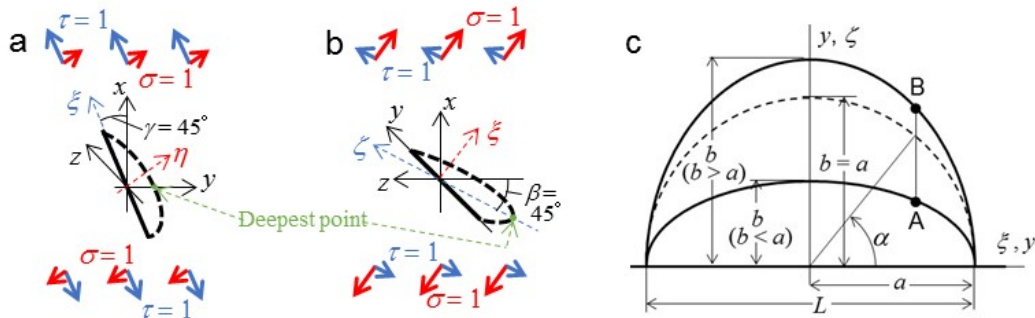


Figure 9: Inclined semi-elliptical surface-cracks in a semi-infinite body subjected to tension load in the x -direction at infinity: (a and b) a model for crack on the ξx - and ξy -planes; (c) the definition of α , and actual position for the ξx - and ξy -plane crack fronts.

at $\alpha = 1^\circ$ instead of $\alpha = 0^\circ$, because in 3-dimensional surface cracks, the point where the crack front intersects a free surface is known as a corner point. The stress singularity at this point is different from that of an ordinary crack [30]. Generally, it has been difficult to obtain smooth distributions of SIFs along the crack front accurately.



Tabs. 1 and 2 show the DL-SIF values of cracks with the aspect ratio, $b/a = 0.38$ ($T/L = 0.189$) for the ξx -plane crack, and 1.1 ($T/L = 0.550$) for the xy -plane crack, which are given from Fig. 6a. The value of F_I for the ξx -plane crack is larger at the crack bottom ($\alpha = 90^\circ$), than at the surface ($\alpha = 1^\circ$). Therefore, it is natural to consider that the crack growth rate toward the inner direction should be larger than that toward the crack length direction in the surface, giving rise to an aspect ratio larger than 1. However, the actual aspect ratio was much smaller than 1. Regarding the value of F_{II} , it was 0.77 at the surface, but it was 0 at the bottom. The large F_{II} value at the surface promotes in-plane shear-mode crack growth. At the bottom, F_{III} takes a value of 0.83, but it seems reasonable to assume that anti-plane shear-mode deformation at the deepest point is negligible for the inward crack growth. Consequently, the ξx -plane crack predominantly propagated at the surface due to in-plane shear-mode deformation, which brings the generation of new SBs and extension of pre-existent SBs around the crack tip areas, producing the aspect ratio much smaller than 1. The tensile-mode deformation reflected by large F_I values should play the role of crack growth. However, by considering a shallow semi-elliptical shape of crack face, it can be expected that the tensile-mode crack growth has negligible effect on the formation of shallow crack face shape. Rather, the tensile-mode deformation might assist shear-mode growth, through the de-bonding of SBs around the crack tip. It was shown that in stress-controlled fatigue tests of UFG Cu corresponding to an LCF regime [20], the crack grows along the direction at an incline of 45° to the loading axis, because of the shear banding induced by the maximum shear stress and SB decohesion process. Under frictionless condition, the growth resistance to shear-mode crack is likely to be smaller than that to tensile-mode crack. It was shown that in conventional grain sized Cu alloys [31], the growth rate of the shear-mode crack is larger than that of the tensile-mode crack, with the same crack length and same stress amplitude.

Type of crack	α (deg)	F_I	F_{II}	F_{III}
ξx -plane crack $b/a = 0.38$	1	0.68	0.77	0.31
	90	0.93	0	0.83

Table 1: Dimensionless stress intensity factors for the ξx -plane crack ($b/a = 0.38, a = L/2$).

Type of crack	α (deg)	F_I	F_{II}	F_{III}
xy -plane crack $b/a = 1.1$	1	0.74	-0.08	0.09
	90	0.60	0.53	0

Table 2: Dimensionless stress intensity factors for the xy -plane crack ($b/a = 1.10, a = L/2$).

For the xy -plane crack (Tab. 2), the F_I value at the surface was 0.74, which is larger than 0.60 at the bottom. This should lead to a superior extension of crack length, compared to the crack depth ($b/a < 1$), if the crack growth was dominantly controlled by the tensile-mode. However, the actual crack extension was accelerated at the bottom, rather than the surface. On the other hand, the F_{II} value was higher at the bottom (0.53) than the surface (-0.08), suggesting that the deep semi-elliptical shape of the xy -plane crack was attributable to the crack extension due to in-plane shear-mode deformation at the bottom. At the surface, mode I crack growth appeared to be predominant, because of negligible values of F_{II} and F_{III} . In addition, the de-bonding of pre-existent SBs in the heavily deformed zone around crack tips occurred due to the tensile-mode deformation, forming a zigzag crack path, as the result of joining the crack and de-bonded SBs. Such a growth path may be convenient for roughness-induced crack closure, which contributes to a decrease in CGR at the surface. It can be concluded, therefore, that mode II crack growth plays an important role in determining the crack face shape of ECAPed UFG copper in LCF regime.

It has been shown that the SBs appear on the ξx -plane at 45° to the loading direction, mainly because it is the plane of maximum resolved shear stress. However, as innumerable planes of maximum shear stress exist, why does only one set of SBs form? To answer this question regarding the formation of only one “family” (one plane and shear direction), Agnew et al. [22] suggested the action of a small sample misalignment. During the full tension-compression of such small samples (2×2 mm cross section), alignment is critical and any deviation would increase the likelihood of the nucleation one type of SBs. Goto et al. [32] monitored the surface of ECAPed copper fatigued by a rotating-bending fatigue machine that has no structural misalignment relating to the nucleation of one type of SBs, showing that SBs were oriented along one set of



maximum shear planes which correspond to the shear plane of the final pressing. Therefore, questions regarding why one type of SBs nucleates, as observed, are still unanswered.

CONCLUSIONS

The main findings of this study can be summarized as follows:

The direction of the crack growth paths strongly depended on both stress amplitudes and crack initiation sites along the circumferential direction of the round-bar specimen. At low stress amplitudes, like conventional grain-sized materials, the cracks grew perpendicular to both the loading direction and specimen surface regardless of the crack initiation sites. At high stress amplitudes, the inclination of crack paths were observed. On the specimen surface, the inclination of the crack paths to the loading direction was 45° in the xz -plane and 90° in the xy -plane, whereas the inner crack path was inclined 90° and 45° to the specimen surface in the xz - and xy -plane crack, respectively. Profile of crack at low stress amplitudes showed the aspect ratio of $b/a = 0.82$ for both plane cracks. At high stress amplitudes, the values of aspect ratios was $b/a = 0.38$ and 1.10 for the xz - and xy -plane crack, respectively. The crack at low stress amplitudes propagated via the striation formation mechanism, which is associated with crack tip retardation and blunting. At high stress amplitudes, however, the formation of crack paths was strongly affected by the in-plane shear-mode deformation and the SB decohesion process around the crack tip areas.

ACKNOWLEDGMENTS

This study was supported by a Grant-in-Aid for Scientific Research (C) (KAKENHI: No. 26420021) from the Ministry of Education, Science and Culture of Japan, as well as a National Research Foundation of Korea (NRF) grant funded by the Korean Government (MSIP) (No.2011-0030058), and by a grant from the Global Frontier R&D Program (2013M3A6B1078874) on Global Frontier Hybrid Interface Materials R&D Center funded by the Ministry of Science, ICT and Future Planning. The authors are very grateful to the members of the Strength of Materials Laboratory of Oita University for their excellent experimental assistance. Thanks are also extended to the members of the Korea Institute of Materials Science, for performing the ECAP processing of our copper rods.

REFERENCES

- [1] Valiev, R.Z., Kozlov, E.V., Ivanov, Yu. F., Lian, J., Nazarov, A.A., Baudelet, B., Deformation behaviour of ultra-fine grained copper, *Acta Metall. Mater.*, 42 (1994) 2467-2475.
- [2] Valiev, R.Z., Structure and mechanical properties of ultrafine-grained metals, *Mater. Sci. Eng.*, A234-236 (1997) 59-66.
- [3] Iwahashi, Y., Horita, Z., Nemoto, M., Langdon, T.G., The process of grain refinement in equal-channel angular pressing, *Acta Mater.*, 46 (1998) 3317-3331.
- [4] Zhu, Y.T., Lowe, T.C., Observations and issues on mechanisms of grain refinement during ECAP process, *Mater. Sci. Eng.*, A291 (2000) 46-53.
- [5] Agnew, S.R., Weertman, J.R., Cyclic softening of ultrafine grain copper. *Mater. Sci. Eng.*, A244 (1998) 145-153.
- [6] Hashimoto, S., Kaneko, Y., Kitagawa, K., Vinogradov, A., Valiev, R.Z., On the cyclic behavior of ultra-fine grained copper produced by equi-channel angular pressing, *Mater. Sci. Forum*, 312-314 (1999) 593-598.
- [7] Vinogradov, A., Hashimoto, S., Multiscale phenomena in fatigue of ultra-fine grain materials-an overview, *Mater. Trans.*, 42 (2001) 74-84.
- [8] Patlan, V., Vinogradov, A., Higashi, K., Kitagawa, K., Overview of fatigue properties of fine grain 5056 Al-Mg alloy processed by equal-channel angular pressing, *Mater. Sci. Eng.*, A300 (2001) 171-182.
- [9] Höppel, H.W., Zhou, Z.M., Mughrabi, H., Valiev, R.Z., Microstructural study of the parameters governing coarsening and cyclic softening in fatigued ultrafine-grained copper, *Philos. Mag. A*, 82 (2002) 1781-1794.
- [10] Wu, S.D., Wang, Z.G., Jiang, C.B., Li, G.Y., Alexandrov, I.V., Valiev, R.Z., The formation of PSB-like shear bands in cyclically deformed ultrafine grained copper processed by ECAP, *Scr. Mater.*, 48 (2003) 1605-1609.
- [11] Mughrabi, H., Höppel, H.W., Kautz, M., Fatigue and microstructure of ultrafine-grained metals produced by severe plastic deformation, *Scr. Mater.*, 51 (2004) 807-812.



- [12] Vinogradov, A., Nagasaki, S., Patlan, V., Kitagawa, K., Kawazoe, M., Fatigue properties of 5056 Al-Mg alloy produced by equal-channel angular pressing, *NanoStruct. Mater.*, 11 (1999) 925-934.
- [13] Chung, C.S., Kim, J.K., Kim, H.N., Kim, W.J., Improvement of high-cycle fatigue life in a 6061 Al alloy produced by equal channel angular pressing, *Mater. Sci. Eng.*, A337 (2002) 39-44.
- [14] Pao, P.S., Jones, H.N., Cheng, S.F., Feng, C.R., Fatigue crack propagation in ultrafine grained Al-Mg alloy, *Inter. J. Fatigue*, 27 (2005) 1164-1169.
- [15] Collini, L., Fatigue crack growth resistance of ECAPed UFG copper, *Eng. Fract. Mech.*, 77 (2010) 1001-1011.
- [16] Meyer, L.W., Sommer, K., Halle, T., Hockauf M. Crack growth in ultrafine-grained AA6063 produced by equal-channel angular pressing, *J. Mater. Sci.*, 43 (2008) 7426-7431.
- [17] Nisitani, H., Goto, M., Kawagoishi, N., A small-crack growth law and its related phenomena, *Eng. Fract. Mech.*, 41 (1992) 499-513.
- [18] Goto, M., Nisitani, H., Fatigue life prediction of heat-treated carbon steels and low alloy steels based on a small crack growth law, *Fatigue Fract. Eng. Mater. Struct.*, 17 (1994) 171-185.
- [19] Zhang, J.Z., A shear band decohesion model for small fatigue crack growth in an ultra-fine grain aluminium alloy, *Eng. Fract. Mech.*, 65 (2000) 665-681.
- [20] Goto, M., Kamil, K., Han, S.Z., Euh, K., Kim, S.S., Lee, J., Fatigue-induced grain coarsening and crack growth behavior in ultrafine grained copper under different loading histories, *Int. J. Fatigue*, 51 (2013) 57-67.
- [21] Zhang, Z.F., Wu, D.S., Li, Y.J., Liu, S.M., Wang, Z.G., Cyclic deformation and fatigue properties of Al-0.7 wt.% Cu alloy produced by equal channel angular pressing, *Mater. Sci. Eng.*, A412 (2005) 279-286.
- [22] Agnew, S.R., Vinogradov, A., Hashimoto, S., Weetman, J.R., Overview of fatigue performance of Cu processed by severe plastic deformation, *J. Electronic Mater.*, 28 (1999) 1038-1044.
- [23] Kunz, L., Lukáš, P., Svpboda, M., Fatigue strength, microstructural stability and strain localization in ultrafine-grained copper, *Mater. Sci. Eng.*, A434 (2006) 97-104.
- [24] Valiev, R.Z., Kozlov, E.V., Ivanov, Yu. F., Lian, J., Nazarov, A.A., Baudalet, B., Deformation behaviour of ultra-fine grained copper, *Acta Metall. Mater.*, 42 (1994) 2467-2475.
- [25] Goto, M., Han, S.Z., Kim, S.S., Kawagoishi, N., Lim, C.Y., Significance of non-equilibrium grain boundaries in surface damage formation of ultrafine-grained copper in high-cycle fatigue, *Scripta Mater.*, 57 (2007) 293-296.
- [26] Mughrabi, H., Höppel, H.W., Cyclic deformation and fatigue properties of ultrafine grain size materials: current status and some criteria for improvement of the fatigue resistance, *Mater. Sci. Res. Symp. Proc.*, (Eds. Farkas, D., Kung, H., Mayo, M., Swygenhoven, H.V., Mughrabi, H., and Weertman, J.), USA, 634 (2001) B2.1.1-12.
- [27] Goto, M., Han, S.Z., Euh, K., Kang, J-H., Kim, S.S., Kawagoishi, N., Formation of a high-cycle fatigue fracture surface and a crack growth mechanism of ultrafine grained copper with different stages of microstructural evolution, *Acta Mater.*, 58 (2010) 6294-6305.
- [28] Xu, C., Wang, Q., Zheng, M., Li, J., Huang, M., Jia, Q., Zhu, J., Kunz, L., Buksa, M., Fatigue behavior and damage characteristics of ultra-fine grain low-purity copper processed by equal-channel angular pressing (ECAP), *Mater. Sci. Eng.*, A475 (2008) 249-256.
- [29] Noda, N-A., Kagita, M., Variations of stress intensity factors of a semi-elliptical surface crack subjected to mode I, II, III loading, *Inter. J. Pressure Vessels Piping*, 81 (2004) 635-644.
- [30] Benthem, J.P., State of stress at the vertex of crack in a half-space, *Int. J. Solids Struct.*, 13 (1977) 479-492.
- [31] Goto, M., Han, S.Z., Kim, C.J., Yamamoto, T., Kawagoishi, N., Crack initiation and small crack growth behavior of age-hardened Cu-6Ni-2Mn-2Sn-2Al alloys, *J. Soc. Mater. Sci. Jpn.*, 53 (2004) 223-229. (in Japanese)
- [32] Goto, M., Han, S.Z., Yakushiji, T., Lim, C.Y., Kim, S.S., Formation process of shear bands and protrusions in ultrafine grained copper under cyclic stresses, *Scripta Mater.*, 54 (2006) 2101-2106.